A Flux Scale for Southern Hemisphere 21cm EoR Experiments

Daniel C. Jacobs[1], Aaron R. Parsons[2], James E. Aguirre[3], Zaki Ali[2], Richard F. Bradley[4,5,6], Chris L. Carilli[7], David R. DeBoer[8], Matthew R. Dexter[8], Nicole E. Gugliucci[5], Pat Klima[5], Dave H. E. MacMahon[8] Jason R. Manley[9], David F. Moore[3], Jonathan C. Pober[2], Irina I. Stefan[10], William P. Walbrugh[9]

ABSTRACT

We present a catalog of broad-band spectral measurements from the Donald C. Backer Precision Array for Probing the Epoch of Reionization (PAPER) in South Africa observed in July and September of 2011. In order to reduce the impact of beam calibration, which proves to be a difficult endeavor for transit telescopes such as PAPER, on the determination of source spectra, we have focused on calibrating sources in a narrow declination range. Since each source follows a nearly identical path through the primary beam, this restriction allows beam calibration to be greatly reduced as a source of error, yielding a dramatic improvement in the accuracy of source spectra measured in the 100–200-MHz band which is receiving renewed attention by experiments seeking to measure 21cm emission from the Epoch of Reionization (EoR). Using beam forming and fringe-rate filtering we measure spectra for Pictor A, which provides a key flux reference for PAPER's EoR power spectrum analysis, as well as 31other sources at nearby declinations. Extrapolating from higher frequency catalogs we set the flux scale in a Monte-C'arlo fit across multiple sources. This fit propagates uncertainty from both catalog and measurement errors. Fitting new spectral models to both catalog and the new PAPER data we find a Pictor A flux model accurate to 2.4%. This accuracy is limited by the uncertainty in the catalog measurements we use to estimate an absolute flux scale, and represents an order of magnitude improvement over previous measurements

[1]School of Earth and Space Exploration, Arizona State U., Tempe, AZ

[2]Astronomy Dept., U. California, Berkeley, CA

[3]Dept. of Physics and Astronomy, U. Pennsylvania, Philadelphia, PA

[4]Dept. of Electrical and Computer Engineering, U. Virginia, Charlottesville, VA

[5]National Radio Astronomy Obs., Charlottesville, VA

[6]Dept. of Astronomy, U. Virginia, Charlottesville, VA

[7]National Radio Astronomy Obs., Socorro, NM

[8]Radio Astronomy Lab., U. California, Berkeley, CA

[9]Square Kilometer Array, South Africa Project, Cape Town, South Africa

[10]Cavendish Lab., Cambridge, UK

in this band. Comparing with prior measurements, 90% are found to confirm and refine a power-law model for flux density.

Subject headings: dark ages, reionization, first stars — catalogs — instrumentation: interferometers

1. Introduction

Numerous radio telescopes are now exploring the prospects for using measurements of highly redshifted 21cm emission to inform our understanding of cosmic reionization in the redshift range $6 < z < 12$, corresponding to radio frequencies below 200 MHz (see reviews in Furlanetto et al. 2006; Morales & Wyithe 2010; Pritchard & Loeb 2012). These include telescopes aiming to measure the global temperature change of 21cm emission during the Epoch of Reionization (EoR), such as the Compact Reionization Experiment (CoRE), the Zero-spacing Interferometer (**?**) and the Experiment to Detect the Global EoR Signature (EDGES; Bowman & Rogers 2010), and interferometers aiming to measure the power spectrum of 21-cm EoR emission, such as the Giant Metre-wave Radio Telescope (GMRT; Paciga et al. 2011, 2013)[1], the LOw Frequency ARray (LOFAR; Yatawatta et al. 2013)[2], the Murchison Widefield Array (MWA; Bowman et al. 2012; Tingay et al. 2013))[3], and the Donald C. Backer Precision Array for Probing the Epoch of Reionization (PAPER; Parsons et al. 2010; Pober et al. 2013)[4].

As such, there has been a renewed interest in the spectral and spatial variation of foreground emission in the 100–200 MHz frequency band that covers the z = 6–13 redshift range expected to encompass reionization (Furlanetto et al. 2006). In particular, the spectral properties of extragalactic point-sources are important both because they are valuable calibration references and because they are strong foreground emitters that must be removed from 21-cm EoR measurements. With the sparse availability of measured foreground properties in the 100–200-MHz frequency band over large areas of the sky (de Oliveira-Costa et al. 2008), continued foreground characterization is a vital step en route to any 21-cm EoR detection. At these low frequencies the Southern sky is much less well known than the North, with catalog source fluxes at 150MHz being inaccurate at the 20% level for $\delta < -20°$(Slee 1995; **?**). Both PAPER and the MWA are located in the southern hemisphere at radio-quiet reserves being prepared for the upcoming Square Kilometer Array, and hence, the most extensive surveying work is now being conducted by the EoR experiments themselves (Jacobs et al. 2011; Williams et al. 2012; Bernardi et al. 2013).

[1] `http://gmrt.ncra.tifr.res.in/`

[2] `http://www.lofar.org/`

[3] `http://www.mwatelescope.org/`

[4] `http://eor.berkeley.edu/`

One significant complication to improving the state of affairs in foreground characterization is that many 21cm EoR experiments, including LOFAR in the northern hemisphere, and PAPER and MWA in the southern hemisphere, are designed for drift-scan observations or steered via phased array. This design decision has largely been driven by the simplicity and cost-effectiveness of phased and/or correlated dipoles to achieve the aggressive sensitivity requirements for measuring the 21cm power spectrum of reionization. Adding to the challenge, these telescopes cover much wider fields of view ($> 10°$) and bandwidths ($\sim 100\%$ fractional) than traditional dish telescopes. Because they do not physically point, flux calibration for such arrays relies heavily on an accurate model of the primary beam response to correct for an the apparent flux scale that varies across the sky. This direction dependent gain is currently uncertain to 10% or higher (Pober et al. 2012), and comprises a large fraction of the 20% difference between current telescopes (Jacobs et al. 2013a).

In this paper, we set out to significantly improve the accuracy of spectral measurements between 100–200 MHz for a set of bright sources in the declination range -46°to -40°that are of particular value for southern-hemisphere 21cm EoR experiments such as PAPER and the MWA. Using the fact that, for this restricted declination range, sources transit through a nearly identical primary beam response pattern, we are able to avoid one of the most debilitating source of error in these measurements: the primary beam. In section **??** we provide some background on uncertainty in early EoR-band catalogs, and explain our choice of calibrator. Section 3 gives an overview of our approach to making the measurement and motivates our data processing steps, which are described in detail in section 4. In section

In section 3 we describe our approach for measuring source spectra with drift-scan observations and deriving an absolute flux scale from catalog data. In §4 we detail the instrumental setup, observations and analysis method followed. Sections **??** through 7 detail our approach for fitting a global flux scale and spectral models for each source. We use these fits in section **??** to understand how well PAPER data agree with previous measurements and conclude in 6.

2. Background

Historically, the best EoR band data were by Slee (1995) with Culgoora Circular Array[5] and various higher frequency measurements with Parkes. These data are typically uncertain to 20% or higher and provide little coverage of the EoR band beyond a single narrow-band data point.

More recent surveys include narrow-band surveys by the GMRT and Mauritius, a deep survey of the region near Hydra A by the 32 antenna MWA prototype Williams et al. (2012) and a wide field survey by PAPER, also with 32 elements Jacobs et al. (2011). Several sub-channels were provided in the Williams catalog, though with 60-80% error bars —large compared to the 30% uncertainty on their wide band measurements. The latter cover the band and spatial scales relevant to EoR

[5]Known during daylight hours as Culgoora Radio Heliograph

measurements but are limited by the accuracy of the primary beam (Jacobs et al. 2013a). The accuracy of the absolute flux calibrators in the southern hemisphere is similarly limited.

The response of the primary beam is of critical importance to EoR measurements. Differences between the polarization responses cause leakage of polarized signals into the total intensity measurement possibly corrupting the EoR power spectrum Moore et al. (2013). The primary beam shape is also critical to measuring and subtracting foregrounds Bernardi et al. (2012) a process which, to be affective, must be done to better than 1% precision for the brightest sources Liu et al. (2009); Bowman et al. (2009) .

A method for decoupling uncertain fluxes from the uncertain beam has been described by Pober et al. (2012). In simulation the method was able to achieve 3 to 10% accuracy in measuring the primary beam, depending on the number of antennae and other variables. The Pober method emphasized the need for many repeated measurements of each alt-az pointing. Further investigation is under way to improve and implement this method and would be greatly aided by the availability of precise flux measurements unaffected by primary beam uncertainty.

In this paper we provide a set of detailed total flux measurements aimed at providing an absolute flux calibration for southern hemisphere EoR studies as well as a small set of verification fluxes suitable for constraining future primary beam studies.

2.1. The sources and instrument

EoR measurements in the southern sky have focused on the coldest regions where galactic foregrounds are minimal. With the majority of possible observing time falling on RA=4h,Dec=-30. The brightest and least-resolved calibrator in this region is Pictor A (5h19m49.1 -45d46m45.0). Pictor A is a nearby FR-II type radio galaxy similar to Cygnus A. At ∼400Jy Pictor is bright and sufficiently distant from other bright sources to make it eminently suitable as both a phase and flux calibrator. Its apparent size of $\sim 8'$is smaller than the scales being probed by current EoR instruments , making resolution effects, making it suitable for precision calibration. However, like most other sources, precise flux measurements in the EoR band are not available. The current best EoR band measurement is uncertain to 12% and appears to imply spectral flattening in the EoR band (Perley et al. 1997).

Establishing an accurate spectrum for Pictor A is of particular importance for PAPER — a dedicated EoR experiment that employs drift-scanning, dual-polarization dipole antennas tuned for efficient operation over a 120–170-MHz band. PAPER is located in the South African Karoo desert on the Square Kilometer Array South Africa (SKA-SA) reserve, 100km north of the small town of Carnarvon. The PAPER array has grown from 16 elements deployed in early 2009 to a 64-element imaging array in 2011 (see Figure 1). Since November 2011 it has been arranged in a maximally redundant grid configuration to make deep power spectral integrations (Parsons et al. 2012). Though highly sensitive as a power spectrum instrument, the maximally redundant array has a broad point spread function in the image domain. This severely limits the number of sources which may be used for flux calibration. Drift scanning across the sky with a 45°FWHM primary beam there are very few unresolved, bright sources which are far from the galactic plane. Pictor A is bright and well enough separated from other emission to dominate the visibilities for a good fraction of the EoR observing season, making it an ideal flux calibrator.

3. Approach

In this section, we describe how we use PAPER in its imaging configuration to measure Pictor A and confirm our results by measuring a selection of known, bright sources. The fluxes are obtained by forming beams towards known sources as they drift through the primary beam, calibrating to a single source making a similar track. These long tracks provide allow us to sidestep primary beam uncertainty to measure accurately calibrated fluxes.

In Jacobs et al. (2013b) several errors were identified as originating in primary beam uncertainty. First, under most imaging schemes, each source flux is measured at just a few points in the primary beam. As errors tend to vary across the beam, the uncertainty will tend to vary between sources making it difficult to decouple flux uncertainty from beam uncertainty. Using the drift scan-beamforming technique, each source is measured hundreds of times at a variety of different pointings to provide a complete sample of the flux variance due to primary beam variation. Second, the flux calibration was found to vary over the sky due to the dual uncertainties of primary beam response and prior catalog. To limit our exposure to flux calibration variation we limit our observations to sources passing within 5°of locations which we can directly calibrate from a single reference source. A third limitation, identified in Williams et al. (2012), was the increase of uncertainty towards the edge of the beam. To minimize our sensitivity to both beam and noise uncertainty, we weight the source track by an additional factor of the primary beam model.

3.1. Selection of confirmation sources

As PAPER is a drift scan instrument, each declination describes a distinct path through the primary beam. These paths provide a detailed sample of the primary beam relative to the peak of the trace, however, a model is still required to calibrate between declinations and the accuracy of the trace is sometimes contaminated by sidelobes. In section XXX we will compare the beam response as measured by the PicA trace with the model used to estimate flux. We will see that, on average, the primary beam is not the limiting factor in estimating the flux and that limiting ourselves to a declination range of 5°around calibrator 2331-416 for flux verification is a good compromise.

We choose sources from the Molonglo Reference Catalog (Large et al. 1981, MRC) that are within 5°in declination of a common calibrator (J2331-416) and have a flux extrapolated from

408MHz greater than 10Jy assuming a power law spectral index of -1.[6] This selection contains 62 sources in a narrow stripe that passes through the majority of the southern EoR fields, much of the galaxy and Centaurus A. This stripe in the broader context of the galactic plane is shown in Figure 15. A list of these sources is given in Table **??**.

For these sources, spectral data measured below 2 GHz were compiled from the NASA/IPAC Extragalactic Database (NED) [7]. Cross-matching radio sources between bands is made difficult by changes in resolution, spectral curvature, and resolved multi-scale structure. For a small number of sources these problems can be ameliorated by inspection of the spectra, source names, coordinates, and originating publications. However for a large sample of sources this becomes unwieldily and prone to error. Thus for the larger number of samples we make use of the Vollmer et al meta-catalog which takes pains to match multi-wavelength observations (Vollmer et al. 2010).

Data Processing Overview

The spectra reported here are measured by beam-forming —phasing the visibilities to the target location and summing to produce a dynamic spectrum. The spectrum is then isolated from neighboring sources by filtering and averaged in the time domain. This time average is weighted by an additional factor of PAPER's primary beam response (Pober et al. 2012).

$$\begin{aligned} S_{\rm est} &= \frac{\sum_t B_M S_p}{\sum_t B_M^2} \\ &= \frac{\sum_t B_M B}{\sum_t B_M^2} S \\ &= g(\delta) S \end{aligned} \tag{1}$$

which is an effective approximation of inverse-variance weighting. The pre factor in Eq 1 is identical for sources at the same declination. In simulation we multiplied an early holographic beam map Pober et al. (2012) by electromagnetic simulations and find that it diverges slowly with declination, with a maximum of 10% over 5°of declination range. We estimate this spectral dependent gain at a reference declination of 41°36′using (J2331-416) fitting a spectral index model to the well-defined data points below 2GHz.

Finally we average the spectra from a resolution of 400kHz to 10MHz bins, adding the individual errors in quadrature as our uncertainty.

At this point we have a set of spectra that have been calibrated relative to each other to the best of our ability. Now they must be put on a global flux scale. Meanwhile, our error estimate

[6] Most radio sources in this band have power law spectra $S(\nu) = \left(\frac{\nu}{\nu_0}\right)^\alpha$.

[7] `http://ned.ipac.caltech.edu/`

does not include an estimate of the flux calibration error. To address both points we fit for a global flux scale that incorporates data from many catalogs. These catalogs have all been set, as best as possible, to the Baars et al scale. Using a Bayesian analysis we compute the variation in the flux scale implied by comparing many sources to prior catalog models. By including sources from across the declination range,the variation in this flux scale fit estimates the overall uncertainty in flux resulting from primary beam or prior catalog uncertainty. Though the final scale is calibrated to the Baars scale, as extrapolated beyond its lower limit of 300 MHz, the flux scale error derived by this method fully describes the error resulting from this extrapolation.

4. Data Reduction

4.1. Observations

Measurements are derived from observations using the east-west dipole arms of 64 PAPER antennas deployed in a minimum-redundancy imaging configuration (see Figure 1) at the Karoo Radio Observatory site in South Africa. A 100-MHz band from 100-200MHz was correlated with 2048 frequency channels and integrated for 10.7 seconds before visibilities were stored. Observations included here on July 4, 2011, running from JD2455748.17 to JD2455748.72. and October 17, 2011 running from JD2455852.2 to JD2455852.6. In both seasons two antennas were omitted owing to malfunctioning signal path. This 20 hour long combined dataset provides observations provides complete hour angle coverage for the entire 24 hours of Right Ascension. The July portion of the dataset comes from the same observing campaign described by Pober et al. (2013) and Stefan et al. (2012).

4.2. Data Compression

In pre-processing, we use delay/delay-rate (DDR) filters (Parsons & Backer 2009) to identify radio-frequency interference (RFI) events, and as part of a data compression technique that reduces data volume by over a factor of 40. A more detailed description may be found in Appendix A of Parsons et al. (2013), which uses the same compression method on PAPER power spectrum observations. Here we summarize the process.

First, we remove known RFI transmission bands and analog filter edges, and then flag outliers at 6σ to remove RFI events. Next, we suppress foreground emission by applying a DDR filter to remove delays and delay-rates within the horizon limit of a 300-m baseline (the maximum length of any PAPER baseline). We derive a second set of RFI flags by masking 4σ outliers in these residuals and apply these flags back to the unfiltered data. Finally, we compress the data by applying a DDR filter preserving emission within the horizon limit of a 300-m baseline, deconvolving to suppress flagging artifacts, and down-sampling the result in time/frequency domain to the critical Nyquist

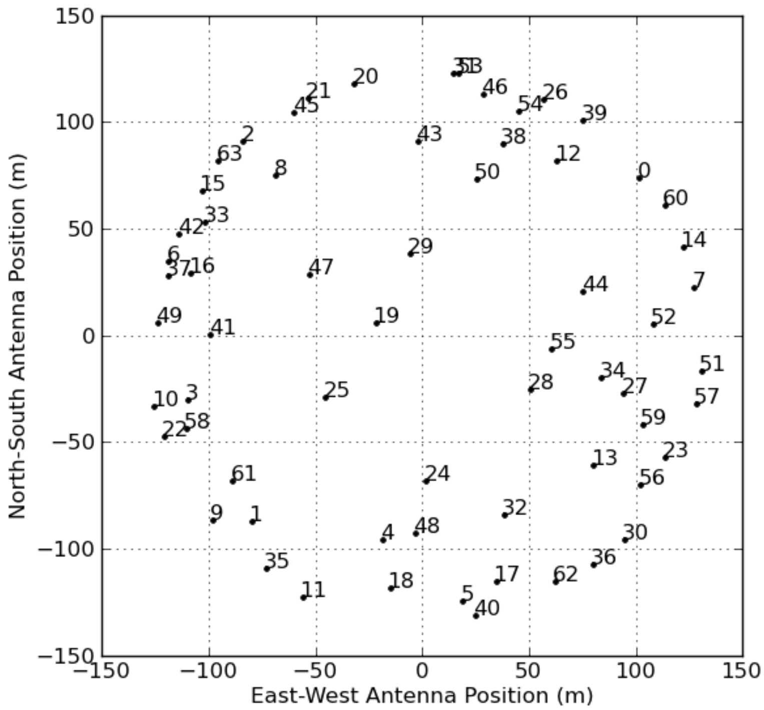

Fig. 1.— Antenna position in the 64-antenna, minimum-redundancy PAPER array configuration at the Karoo Radio Observatory site in South Africa used for these observations. Data was captured during July and October of 2011 on a single 'x' polarization over a band between 120 and 180 MHz.

rate of the DDR filter. The result is that the 2048 original frequency channels become 203, and the 60 original time samples per 10-minute file become 14.

4.3. Per-Antenna Gain Calibration

Small gain variations between antennae and over time introduce significant systematic effects which degrade instrument performance. Temporal variations are dominated by changes in ambient temperature. Measurements of ambient temperature versus time near the balun amplifier of a fiducial antenna and near receiver amplifiers were used to divide out the predicted gain variation versus temperature that these amplifiers are known to exhibit. Inspecting the auto correlations we find that the net temperature gain coefficient (-0.042 dB/C) found in previous laboratory Parashare (2011) and early field measurements Pober et al. (2012) did not appear to remove all temperature variation (black curve in Figure 3). To revise the temperature coefficient we use the October observations, when the temperatures remained nearly constant, as a reference.

Comparing the average ratio between the July and October autocorrelations to their temperature difference (Figure 2) we find that the two are highly correlated with a best fit temperature coefficient of (-0.058 dB/C). As we see in the Figure 3, this removes a significant amount of disagreement between the two nights, with the peak difference decreasing from 18% to 3%.

Matching of relative gains and phases between antenna was done by fitting a per-antenna complex gain to portions of data which have easily modeled sky. This calibration is only relative between antennae, absolute flux calibration comes after time and frequency averaging in §4.7. The antenna delays and amplitudes were found by fitting a point source visibility model to Centaurus A, Pictor A, and Fornax A. Each source is imperfectly modeled by a single point-source, but the solution differences are minimized by averaging over the three independent solutions. These same calibration solutions have been successfully applied in Pober et al. (2013) and Stefan et al. (2012). for power-spectrum analysis of foregrounds and imaging of Centaurus A, respectively.

4.4. Beamforming

Spectral time-series are computed by beam-forming to the selected sky locations. A beam is formed by phasing baselines to the desired location and summing over baselines longer than 20 wavelengths.

These complex spectra are then fringe rate filtered to remove spectrally smooth sources that deviate more than ± 0.1mHz from the fringe rate of the source in question (Parsons & Backer 2009) (cf the LOFAR de-mixing approach Offringa et al. (2012)) producing a time dependent spectrum with minimal side lobes. This is then averaged in time, weighting by a model of the primary beam as discussed above. The result is equivalent to a very long earth rotation synthesis image with a

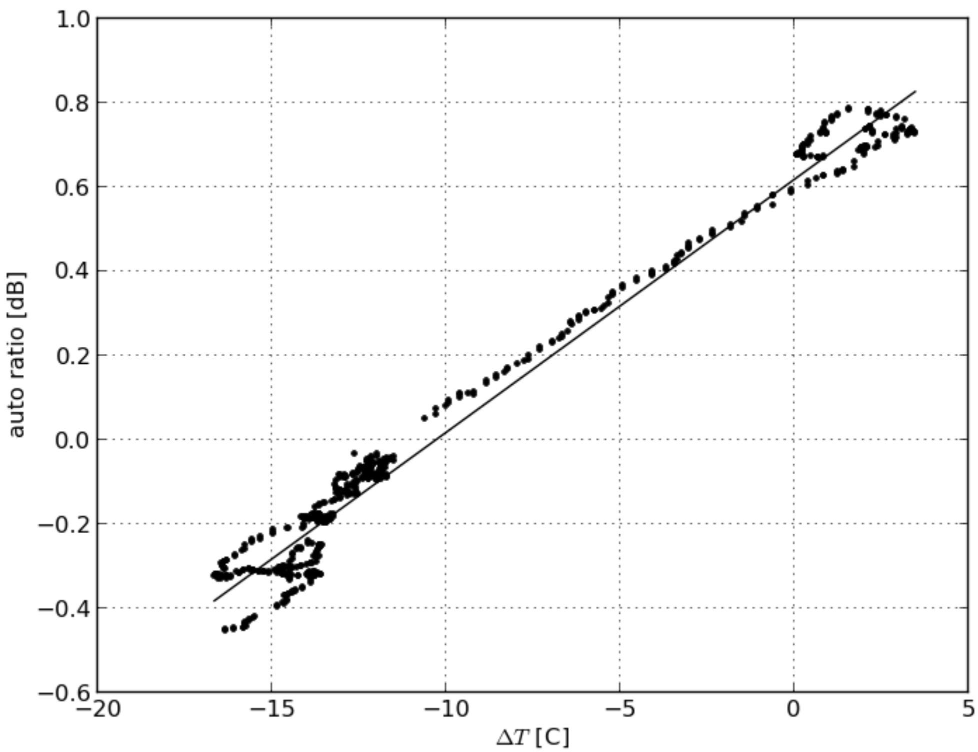

Fig. 2.— Calibrating the temperature coefficient by comparing the two nights. Here we plot the ratio of auto-correlations (averaged over frequency and antenna) against the temperature difference between the two data sets. The very linear middle region has a slope of -0.055 dB/C while the full, more complex, range is fit by -0.06dB/C (black line). We compromise by choosing -0.058dB/C.

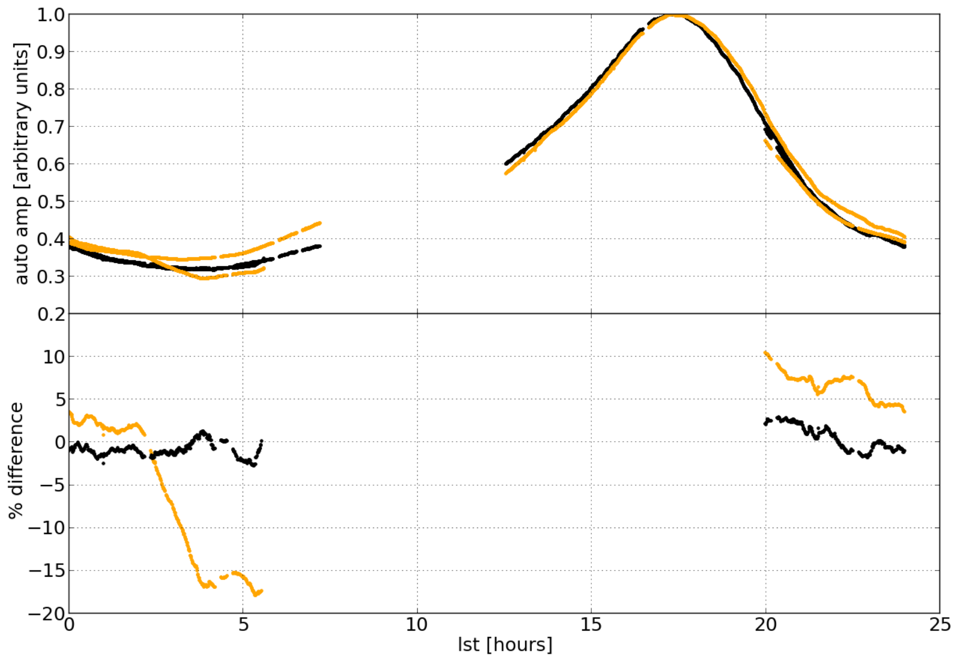

Fig. 3.— Gain differences between the July and October nights are dominated by temperature variation. Here we see the affect on the average auto correlation before (orange) and after (black) application of the temperature dependent gain.

single image pixel. The weighted contributions from each baseline are shown in Figure 4.When combined with the filtering it is a robust and simple method for measuring spectra of unresolved sources.

4.4.1. *Compensation for Resolution Effects in Pictor A*

The beam-forming method assumes the target is a point source. Our primary target, Pictor A, is slightly resolved by PAPER, and merits closer attention. Pictor A is a double-lobed radio galaxy with a main lobe separation of $7'$. As we see in Figure 5, it is nearly unresolved by PAPER's $15'$synthesized beam. However, given the high SNR of the observations, we see a 20% drop in flux on the longest ($\sim$300m) baselines. We account for this by weighting baselines in the beamform step according to a model of structure observed by Perley et al. (1997) at 330MHz, which they found to be consistent with their more limited 74MHz images as well as the detailed high frequency maps. The normalized image is Fourier transformed and sampled at the desired uv spacing by spline interpolation. These samples are used to weight each baseline contribution in the baseline sum. The result is an estimate of the total integrated flux for Pictor A. Where the resolution is highest, at the top of the band, the correction is 3%. At the bottom of the band, where the resolution size has grown to $19'$, the correction is only 0.6%. The resulting spectrum is shown in Figure 8a.

4.5. Bandpass Calibration

The resulting set of spectra were then calibrated to a model of J2331-416 to remove the residual bandpass due to the net effect of the primary beam as discussed in §3. J2331-416 [8] a somewhat arbitrary fit to measurements below 1GHz (Slee 1995; Kuehr et al. 1981; Large et al. 1981; Burgess & Hunstead 2006). was selected for its relatively high brightness, spectral smoothness and large quantity of available catalog data. Each source track has a slightly different sample profile resulting from different amounts of flagged data at each time and channel. To account for these differences in the bandpass calibration we build a set of calibration tracks that match the tracks for each source. Calibration of each source then proceeds with an optimally matched calibration spectrum.

4.6. Fitting a Power-Law Model to Spectra

There is a variety of prior data at multiple wavelengths to which we want to calibrate and then compare our measurements. Our method for doing both of these steps is to assume a basic spectral model relating the different catalog data points and fit for spectral model and gain parameters.

---

[8]Here we set the spectrum to $S_{150} = 33$Jy, $\alpha = -0.76$

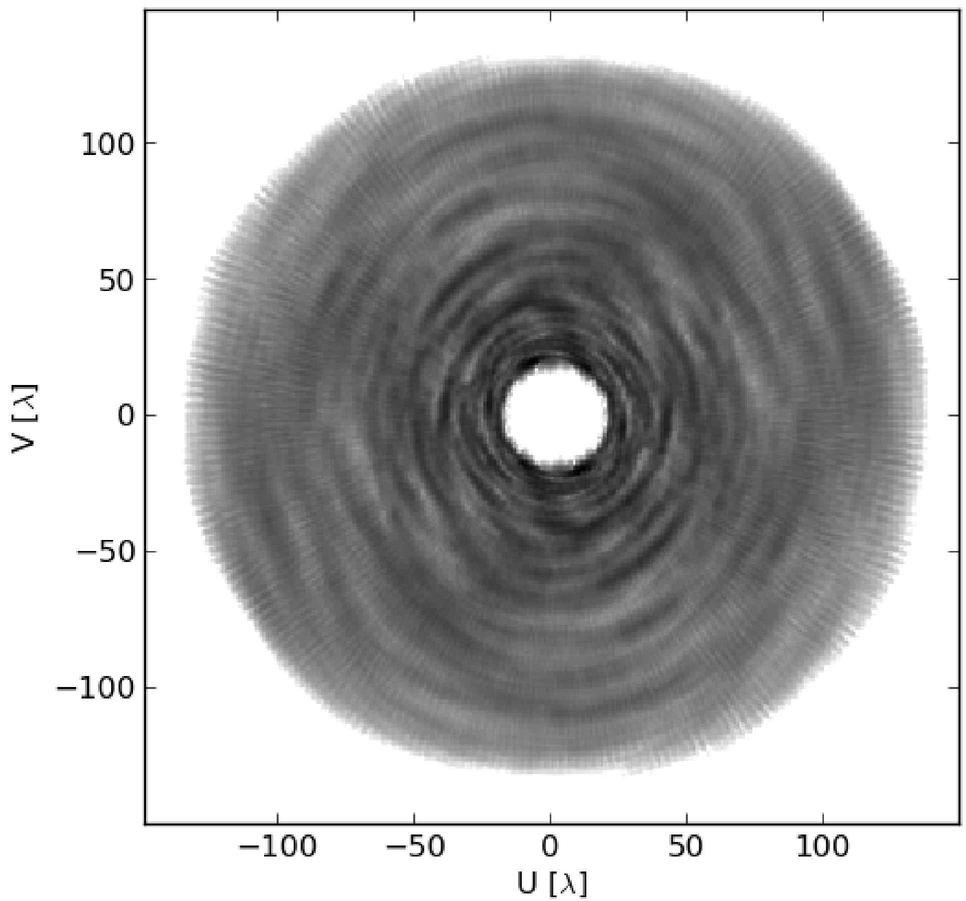

Fig. 4.— The effective uv coverage of a 10MHz-wide spectrum bin, showing the relative contributions of each baseline when beam-forming on Pictor over a 9.6 hour synthesis in the October observing session.
Not shown here are the weights interpolated from the Perley et al 330MHz map (Fig. 5) used to recover the total integrated flux of Pic which represent a few % change on the longest baselines.

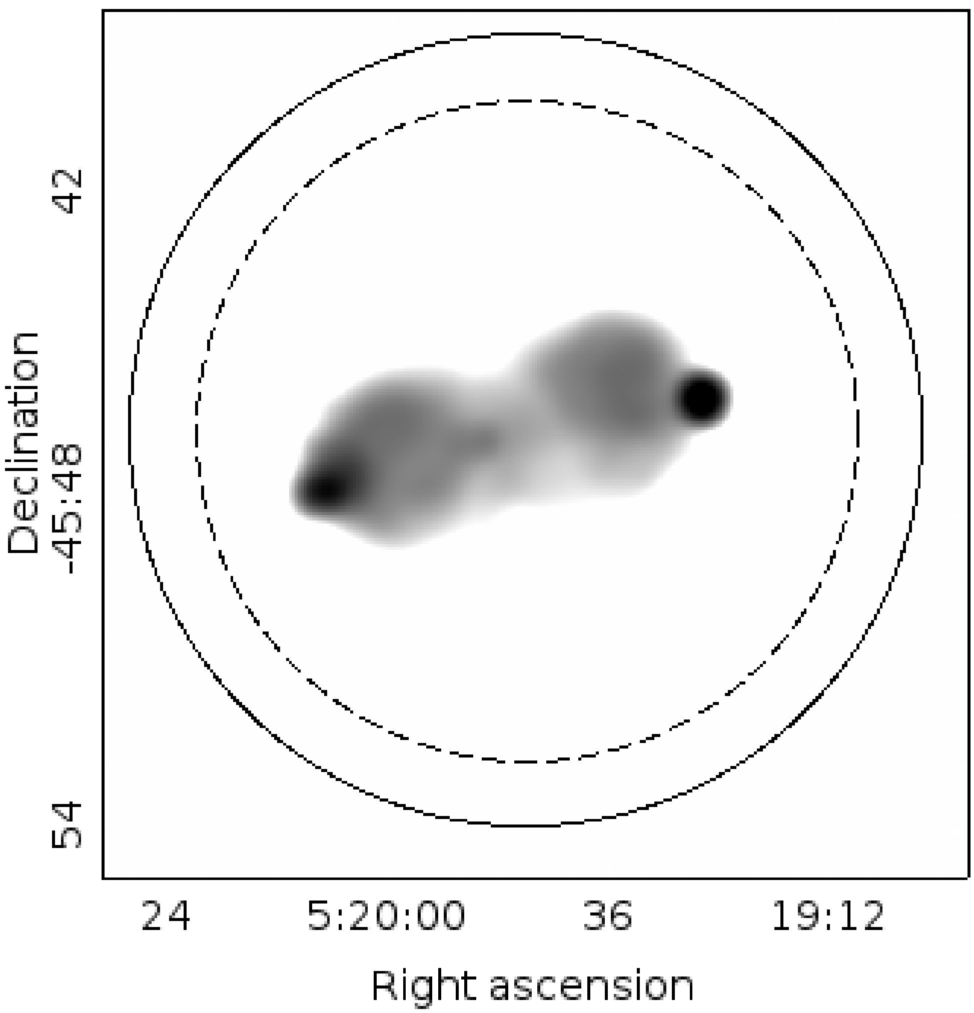

Fig. 5.— Pictor A imaged at 330MHz by the VLA (Perley et al. 1997). Black circle indicates PAPER resolution at the 150MHz, dashed, the resolution at 185MHz. To correct for the small residual structure in the PAPER measurements we resampled the Perley image to the PAPER resolution and estimated the relative contribution to each PAPER baseline. At the highest frequency this led to a 3% correction, at the lowest frequency, 0.6%.

We estimate spectral model parameters and flux calibration in a Bayesian way by calculating and marginalizing the posterior probability of the catalog and new PAPER data. This method offers improved repeatability by specifying a single objective function that represents the quality of the model fit and naturally defines the errors on the parameters (Hogg et al. 2010). See Mackay (2003) or Sivia & Skilling (2006) for more on Bayesian analysis methods and an excellent astrophysical example by Press (1997). In brief, measurement errors are related to parameter model errors via the likelihood, which we can calculate, and the posterior, which we cannot. However, the posterior is theoretically well sampled by a Markov Chain Monte Carlo sampler, which selects parameter values at random, computes the likelihood of the model given the data and noise model, and accepts or rejects the step based on an outside decision factor unrelated to the data.

Here we use the *emcee* sampler by Mackay (2003) et al to generate chains of parameter values. The best fit model is the median of all the sampled parameter sets, while the volume containing a well defined fraction of samples sets the confidence limits. The oft quoted "1σ" probability level corresponding to a gaussian distribution contains 65% of the samples. In practice the contours are not gaussian. Here we choose a slightly more conservative probability level of 76%

To model the relationship between different wavelengths we assume a single spectral index which is the prevailing spectral energy distribution at low frequencies, though curvature or other deviation from a power-law is not-uncommon.

When fitting models to the full catalog, we use the Vollmer et al catalog which has been optimally cross-matched at the expense of excluding more data points. Meanwhile, the gain fit used a small sample of sources with spectra which meet our calibration criteria: more precision data available, brighter than most sources in the sample and far from any possibly confusing areas of the sky. By limiting ourselves to a small number of sources we are able to go include catalog points by hand, to avoid making the error of falsely including erroneously matched data points but benefiting from some measurements not included.

4.7. Approximating an Absolute Flux Scale

At the output of the beam forming and bandpass calibration step, the flux scale is tied to a model fit of the catalog values of J2331-416. The accuracy of this fit, and the implied uncertainty in the flux scale, limits the accuracy of the PAPER measurements.. To refine the flux scale and estimate our flux scale uncertainty, we bootstrap a single global flux scale correction factor using 5 sources selected for their brightness, spectral linearity and data availability[9]. To build a more complete spectral model we go beyond the data found in Vollmer et al, including all spectral measurements below 2GHz found in the NED database [10]. These catalog measurements are primarily

[9]Calibration sources: 2250-412,2331-416,2140-434,0007-446,0704-427

[10]`ned.ipac.caltech.edu`: Accessed 1 April 2013

by Parkes, and Molonglo with the best precision coming from the Wills fluxes at 538 and 634 MHz (when available). Where error bars are not given, we assume uncertainty of 25%.

Using the MCMC method we fit spectral index models to the catalog fluxes simultaneously with a global PAPER flux scale factor using an MCMC chain to calculate the log likelihood

$$\begin{aligned}\log \mathcal{L}_s &= \sum_\nu \frac{\left[S^\nu_{\rm cat} - S_{150}\left(\frac{\nu}{150}\right)^\alpha\right]^2}{2(\Delta S^\nu_{\rm cat})^2} + \frac{(gS^\nu_{\rm PAPER} - S_{150}\left(\frac{\nu}{150}\right)^\alpha)^2}{2(\Delta S^\nu_{\rm PAPER})^2} \\ \log \mathcal{L} &= \sum_s \log \mathcal{L}_s \end{aligned} \tag{2}$$

which samples the posterior probability of PAPER data ($S^\nu_{\rm PAPER}$) and catalog values ($S^\nu_{\rm cat}$) given a spectral index model for each source and a global flux scale factor (g). Marginalizing over the fitted flux scales, we find the resulting flux scale distribution function which is shown in Figure 7. The 76% confidence limit on this flux scale, relative to the J2331-413 calibration, is $+0.11^{+0.05}_{-0.08}$ dB, or a 1.54% multiplicative error on every calibrated PAPER measurement. This flux scale is applied to the PAPER spectra with the errors added in quadrature.

These calibrated spectra are plotted in Figures 9,**??**, & **??** and the data are listed in Table 1. The resulting Pictor A spectrum ranges in precision from 6.5% at 125MHz to 4.7% at 185MHz. At least half of this error is due to uncertainty in the flux scale.

4.8. Fitting Spectral Models

Finally we compare all of our calibrated spectra to catalog measurements. Our method will be to first establish a best fit model to existing data, then add the PAPER data to the fit, and assess the degree to which the PAPER data is supported by prior measurements, or the reverse the degree to which PAPER offers an improvement in our knowledge of the spectrum.

To establish the baseline model, we fit a spectral model to catalog data from the spectrally and spatially cross-matched meta-catalog by Vollmer et al. (2010) using the (log) likelihood which assumes Gaussian measurement errors

$$\log \mathcal{L} = \sum_\nu \frac{\left[S_\nu - S_{150}\left(\frac{\nu}{150}\right)^\alpha\right]^2}{\Delta S_\nu} \tag{3}$$

We estimate the confidence interval of the resulting parameters as the boundary enclosing 76% of the samples. In the catalog we report both the upper and lower of these values for both parameters and plot the 2D contour to show the correlation of the two parameters. Many of these contours, the grey curves in Fig. 10, are classic banana plots, displaying a non-linear correlation between the parameters. In most cases the single contour adequately describes 2D posterior distribution.

Confidence contours for the complete set are shown in grey in Figs. 10 - 11. In general these are lower limits on the possible precision, as the Vollmer catalog emphasizes minimization of cross-match error but at the cost of excluding data points. The fit is then performed again with both PAPER and catalog data, shown in black on the same Figures. The values are given in Table 2, and illustrated in Figure **??**.

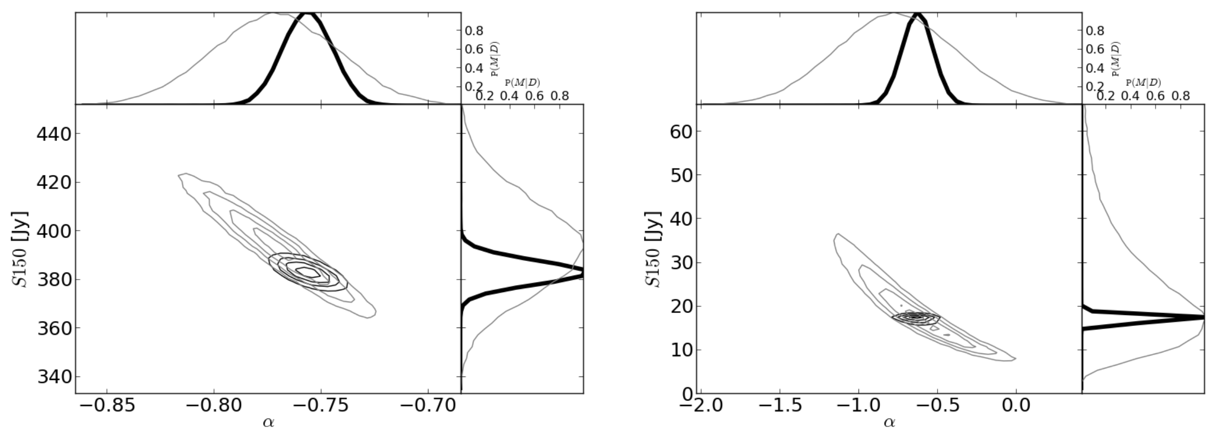

Fig. 6.— A more detailed view of the posterior probability distribution. On the left Pictor A, on the right 2323-407. Confidence contours range from 0.2 to 0.8. The MCMC chain reveals the distinctive "banana" shape of the posterior due to correlation between the model parameters. Compare with the contours for this source shown in Fig. 11. Grey plots the fit to catalog data, black for joint catalog and PAPER.

5. Results and Discussion

The majority of the 32models fit using the new PAPER data were found to agree with models fit to past data and all but two are suitable for comparison. 0008-421 was not detected by previous PAPER observations and exhibits flattening at higher frequencies, most likely due to synchrotron self-absorption (Jacobs et al. 2011). While 1459-417 does not have enough measurements in the Vollmet et al catalog on which to build a model for comparison. We exclude these two from further analysis.

Inspecting the remaining 29 confidence contours we find that, for the vast majority ($\sim 90\%$), the PAPER measurements confirm the power law extrapolation from higher frequencies. The remaining 10% either A) have large PAPER error bars and therefore provide no new information or B) do not agree with the spectral index model. To understand where most measurements fall on this spectrum we numerically quantify the overall model improvement derived from the addition of the PAPER data as

$$\begin{aligned} \text{Improvement} &= (\text{Precision increase})\,(\text{Catalog agreement}) && (4)\\ &= \left(\frac{1}{\text{Area(PAPER)}} - \frac{1}{\text{Area(Cat)}}\right)(\text{Area}(\text{PAPER} \cap \text{Cat})) && (5) \end{aligned}$$

where the area is defined as the number of samples having posterior probability above 76%.

We quantify the fit *precision increase* as the change in the contour figure of merit, defined as the inverse area of the confidence contour. Meanwhile, *catalog agreement* is the fraction of the PAPER confidence interval that overlaps the catalog confidence interval. Thus, for example, in a PAPER fit that overlaps the catalog confidence contour by 41% but increases in precision (confidence area shrinks) by a factor of 3, the resulting *improvement* will be 0.123. This Improvement Index is included in the table of fit parameters (Table 2).

In these sources, the improvement index ranges from a maximum of 7.84 to -0.001. One source (1017-421) shows a slightly negative improvement, suggesting that PAPER data have added to uncertainty (see Figure 14), while two sources have exactly zero improvement, which indicates that the PAPER data have pulled the fit far from the model preferred by the catalog data (see Fig. 13).

However, the vast majority of sources (90%) have positive improvement index, indicating strong confirmation of the extrapolated spectrum (see Figures 10 - 12). Pictor A is in the middle of this group with an improvement of 0.942 —only two sources show stronger confirmation. The flux model is $S150$ =381 ± 5.36Jy, $\alpha = -0.76 \pm 0.01$. The combination of several independent PAPER data points near 150MHz with previous catalog measurements results in this estimated uncertainty of 1.4%. This uncertainty is quite small, but is not surprising when we consider that we have used 7 precise data points (5 PAPER, 2 Wills), all accurate to 3% to measure what appears to be an extremely linear power law spectrum. If the errors were completely guassian the net error would be $3/\sqrt{(7)} = 1.14\%$.

6. Conclusion

Here we have provided a measurement of Pictor A with enough precision to confirm a highly linear spectral index between 150 and 600MHz. We then used the same filtered beam form method to measure the spectra of bright sources with similar primary beam response. This primary beam limit is based on our measurements of the primary beam along slices of constant declination.

The measurements provided here are the first, calibrated, broad-band spectra to cover the EoR band. Existing EoR band measurements are accurate to 20% implying a 40% uncertainty in the absolute power spectrum level. The Pictor A spectrum here is shown to be accurate to ∼5%, a factor of 5 improvement over previous measurements.

This uncertainty includes the variation in each PAPER measurement ($\sim$1%), variation between sources and the errors resulting from extrapolating the Baars et al. (1977) scale beyond its original range. These last two are found simultaneously by fitting the spectral extrapolations of several flux calibrators at once and account for the the majority of the error. Though past measurements suggested the possibility of spectral curvature below 200MHz we have found no evidence for this. With these measurements we are able to confirm single spectral index model for Pictor between 120MHz and 600MHz.

A set of 61 verification sources were selected to be bright, previously cataloged and distributed over the full 24 hours of Right Ascension coverage but only within 5 degrees declination of Pictor A. Using a Bayesian analysis we conclude that most of these are consistent with previous measurements and provide useful new constraints. However, in a small remainder, the simple spectral model fails to adequately describe the data. In most cases the proximity to bright or extended structures implies side lobe contamination. Therefore, though we include the model parameters, they are not meant to be definitive, but provide confidence that the reported PAPER flux values are on the correct global scale.

Direct measurements of the Pictor A spectrum are key to correctly setting the flux scale of PAPER, MWA and future EoR experiments like the Hydrogen Epoch of Reionization Array (HERA). These spectra provide tighter constraints on many of the EoR band fluxes, while limiting the pernicious affect of primary beam uncertainty. Future work will use these fluxes to further refine the primary beam models of these experiments which is crucial to properly reconstructing both image and power spectrum flux.

Acknowledgements

The PAPER project is supported by the National Science Foundation (awards 0804508, 1129258, and 1125558), and a generous grant from the Mt. Cuba Astronomical Association.

This work makes use of]the “MCMC Hammer” emcee python library (Foreman-Mackey et al. 2012, `http://danfm.ca/emcee/`) and the NASA/IPAC Extragalactic Database (NED) which is operated by the Jet Propulsion Laboratory, California Institute of Technology, under contract with the National Aeronautics and Space Administration.

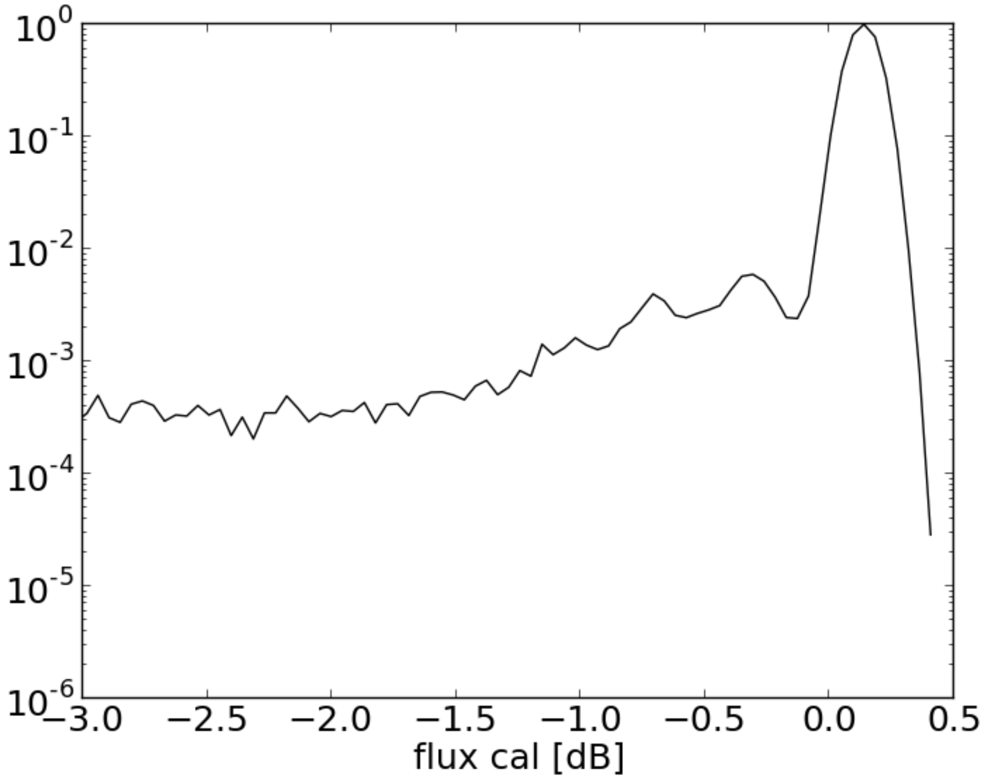

Fig. 7.— The marginalized posterior of the PAPER flux scale factor relative to 2331-416. Given a joint fit to all the NED database listings for 2250-412,2331-416,1932-464,0103-453,0547-408,0043-424 below 2GHz and the corresponding PAPER values. The 76% confidence interval on this distribution is used to set the overall flux scale. While the width is an additional fractional error to be added quadratically to the per-source uncertainty. By averaging over many sources and and Baars calibrated data points, this uncertainty encapsulates error due to both primary beam model inaccuracy as well as the average flux scale uncertainty due to extrapolating many absolutely calibrated measurements.

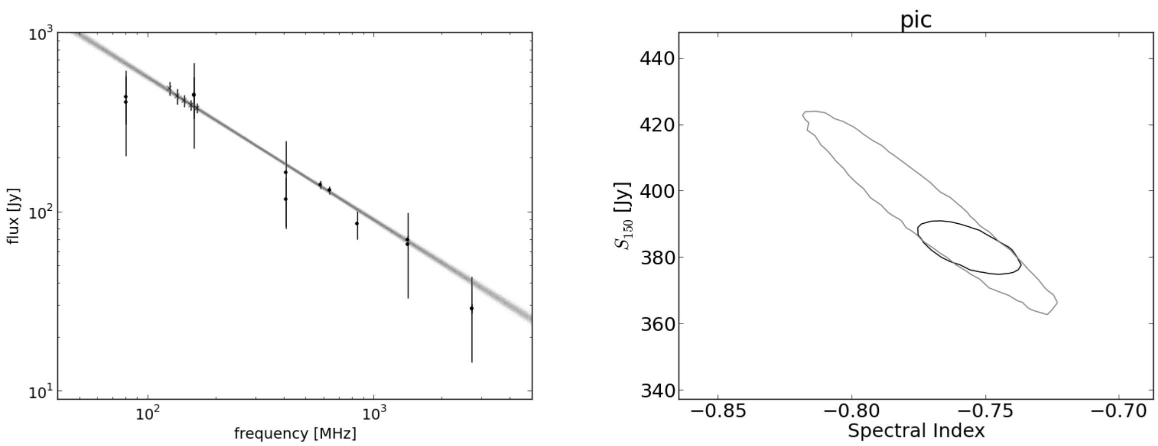

Fig. 8.— Using new PAPER results to constrain the spectrum of Pictor A. On the left, the PAPER Pictor A spectrum with 2σ error bars (x) and MCMC fits (grey cloud). Inset allows comparison between the 10MHz averaged points with the 403kHz points (grey). The oscillations in the PAPER spectrum are residual side lobe contamination from other sources and are well represented by the error bars. The most reliable prior measurements (dots) are those by Wills (1975) at 580MHz and 635MHz (Perley et al. 1997). The rest are from with Culgoora Slee (1995) or Parkes Otrupcek & Wright (1991) and have been set to the (extrapolated) Baars et al. (1977) scale by Kuehr et al. (1981). A sub-sample of MCMC fits are shown in grey. On the right, the grey contour indicates the 76% confidence interval for 150MHz flux and spectral index given the prior data. Black folds in the PAPER data.

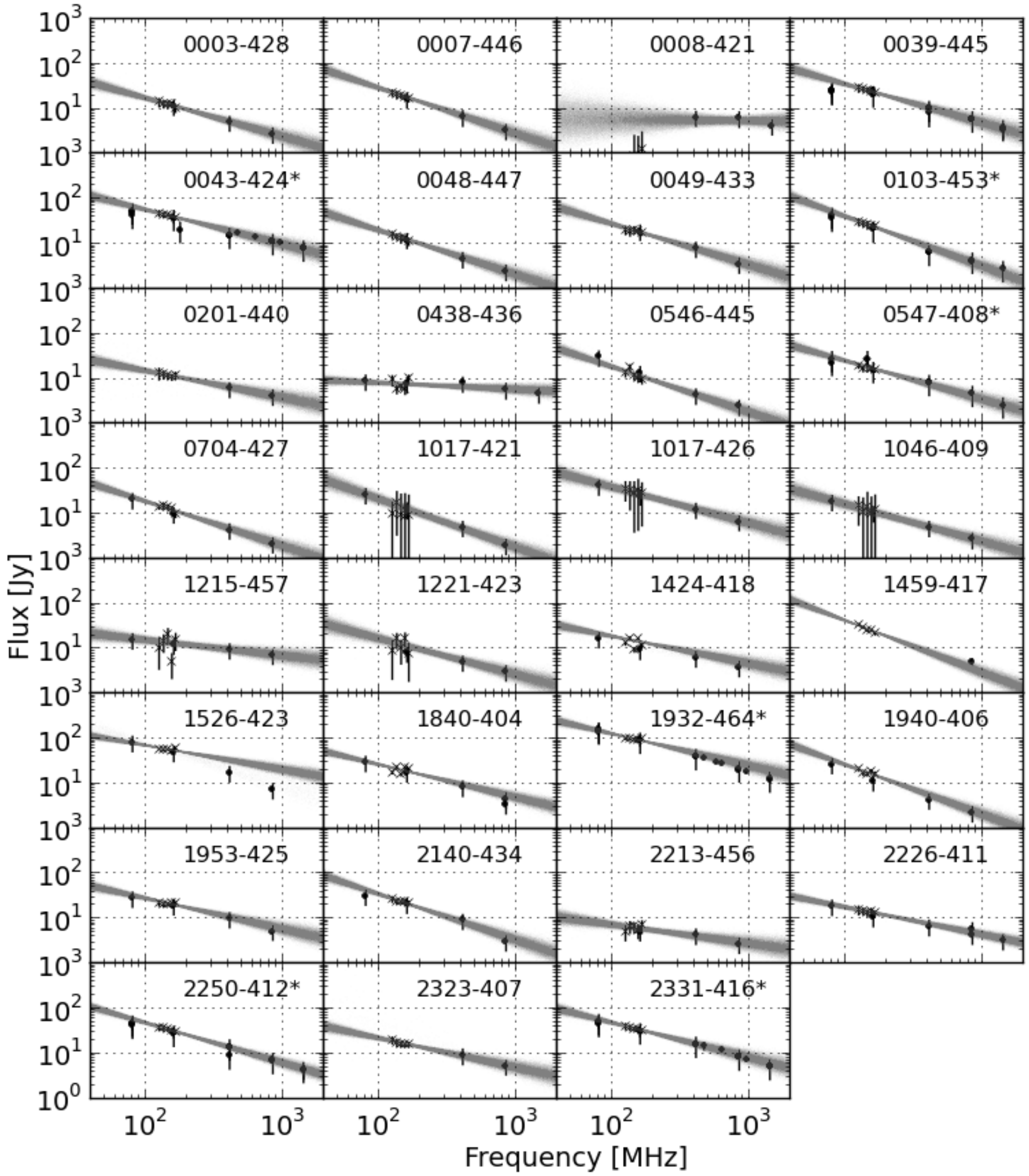

Fig. 9.— PAPER spectra of 16 sources compared against existing data out of Vollmer et al. (2010) between 40MHz and 2GHz, otherwise as described in Figure 8.. Sources used to bootstrap the flux calibration are noted with a * and are shown with the additional calibration data found in NED. Pictor A is shown separately in Figure 8.

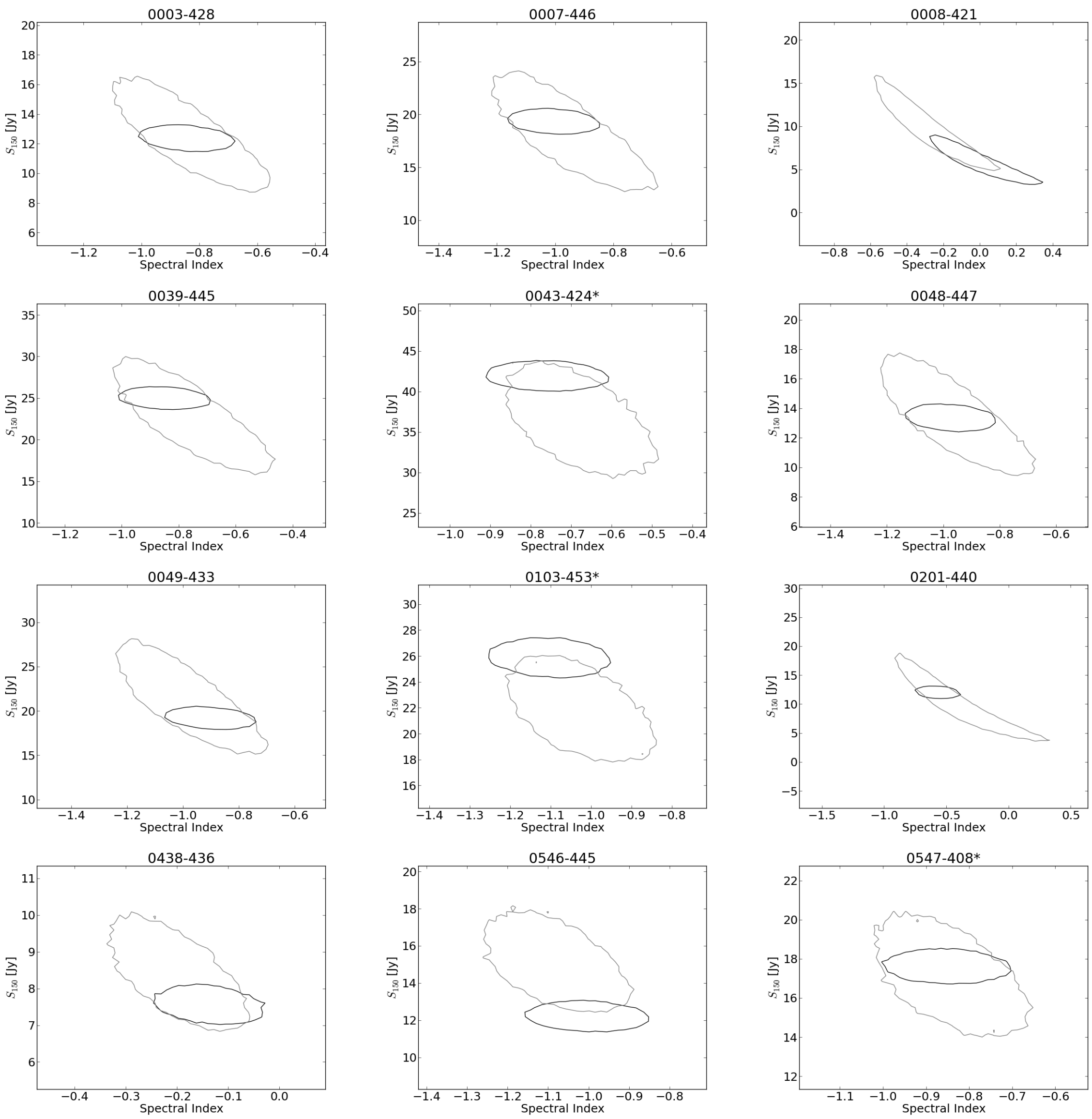

Fig. 10.— Spectral model contours as described in Figure 8. Sources marked with a * were used to assess calibration error.

2

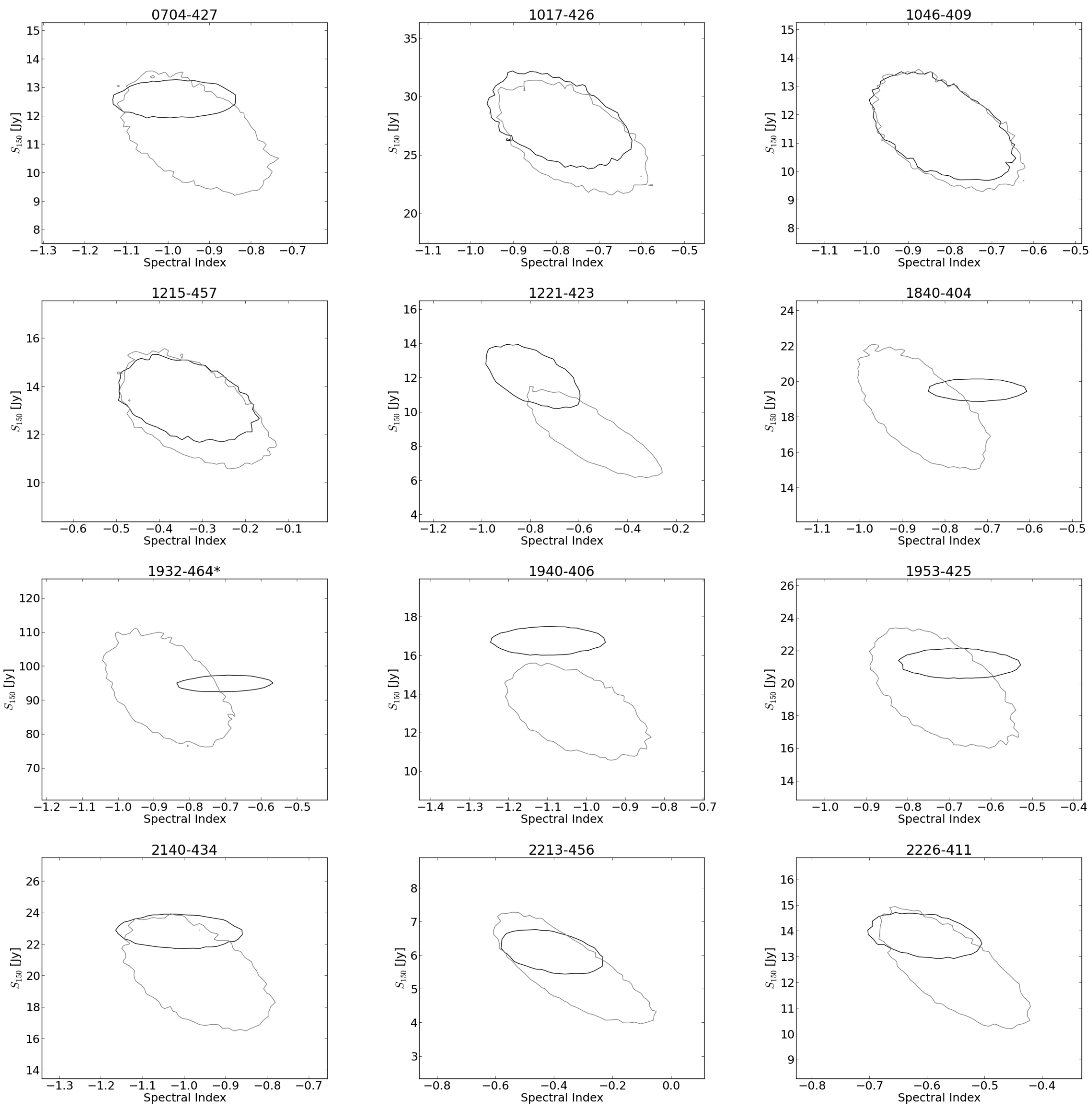

Fig. 11.— Spectral model contours as described in Figure 8. Sources marked with a * were used to assess calibration error.

2

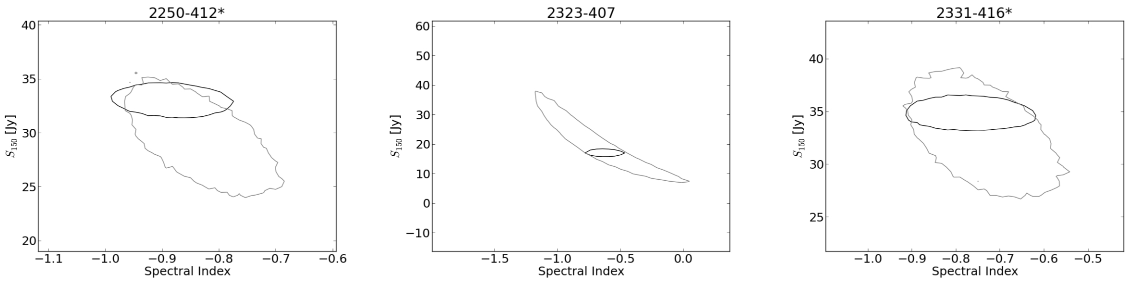

Fig. 12.— fits of the next 16 sources, as described in Figure 10. Sources marked with a * were used to assess calibration error.

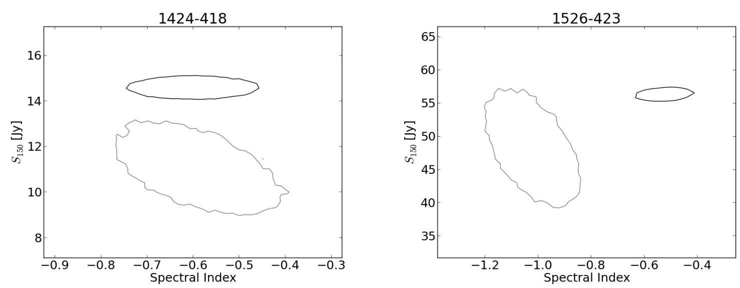

Fig. 13.— These fits are somehow at odds with other measurements. The 1526-42 spectrum is visibly curved (see Fig. 9), which explains the large disagreement in spectral index but not flux. 1424-418 is an optically polarized quasar with a flat and variable radio spectrum which might imply co-aligned jet viewing and high intrinsic variability.

REFERENCES

Baars, J. W. M., Genzel, R., Pauliny-Toth, I. I. K., & Witzel, A. 1977, Astronomy and Astrophysics, 61, 99, a&AA ID. AAA020.141.048

Bernardi, G. et al. 2013, arXiv, astro-ph.CO

—. 2012, ApJ submitted

Bowman et al. 2012, PASA, submitted

Bowman, J., Morales, M., & Hewitt, J. 2009, The Astrophysical Journal, 695, 183

Bowman, J. D. & Rogers, A. E. E. 2010, Nature, 468, 796, (c) 2010: Nature

Burgess, A. M. & Hunstead, R. W. 2006, The Astronomical Journal, 131, 100

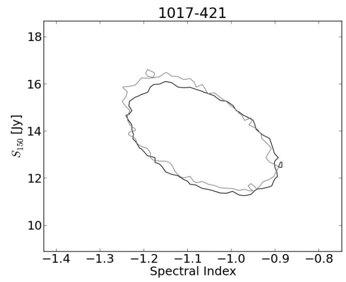

Fig. 14.— A source with a slightly negative improvement index (-0.0011). Here the PAPER data represents a large fraction of the available data but due to the large error bars slightly increases the uncertainty.

Table 1. PAPER spectra for 32 MRC sources

Name	Ra deg	Dec deg	S125 Jy	rms Jy	S135 Jy	rms Jy	S145 Jy	rms Jy	S155 Jy	rms Jy	S165 Jy	rms Jy
Pictor A	80.09	-45.78	455.3	13.3	409.6	15.8	389.2	12.4	363.5	11.1	350.6	9.1
0003-428	1.68	-42.5	14.5	1.7	13.1	1.4	12.8	1.2	12.6	1.1	10.3	1.0
0007-446	2.8	-44.3	23.2	2.2	21.1	2.2	20.2	1.7	18.6	1.4	17.2	1.6
0008-421	2.89	-41.81	-0.2	0.8	-0.3	1.0	0.9	0.9	0.7	0.9	1.3	1.0
0039-445	10.7	-44.16	29.2	3.0	27.6	2.2	26.4	2.2	24.0	1.6	22.2	1.5
0043-424	11.73	-42.05	48.6	4.2	45.2	3.5	43.9	2.3	40.8	2.2	38.4	2.4
0048-447	12.87	-44.4	16.2	1.7	14.6	1.3	13.7	1.6	13.3	1.3	11.3	1.2
0049-433	13.22	-43.03	20.9	2.5	19.0	2.2	20.8	2.2	19.0	1.5	17.4	1.2
0103-453	16.48	-45.02	31.3	3.0	29.0	2.7	27.1	2.9	25.4	1.8	24.3	2.0
0201-440	31.05	-43.76	13.6	2.2	12.6	1.5	11.7	1.0	11.0	1.0	12.0	1.2
0438-436	70.17	-43.53	9.5	1.4	6.0	0.7	6.6	0.6	5.8	0.7	10.5	1.0

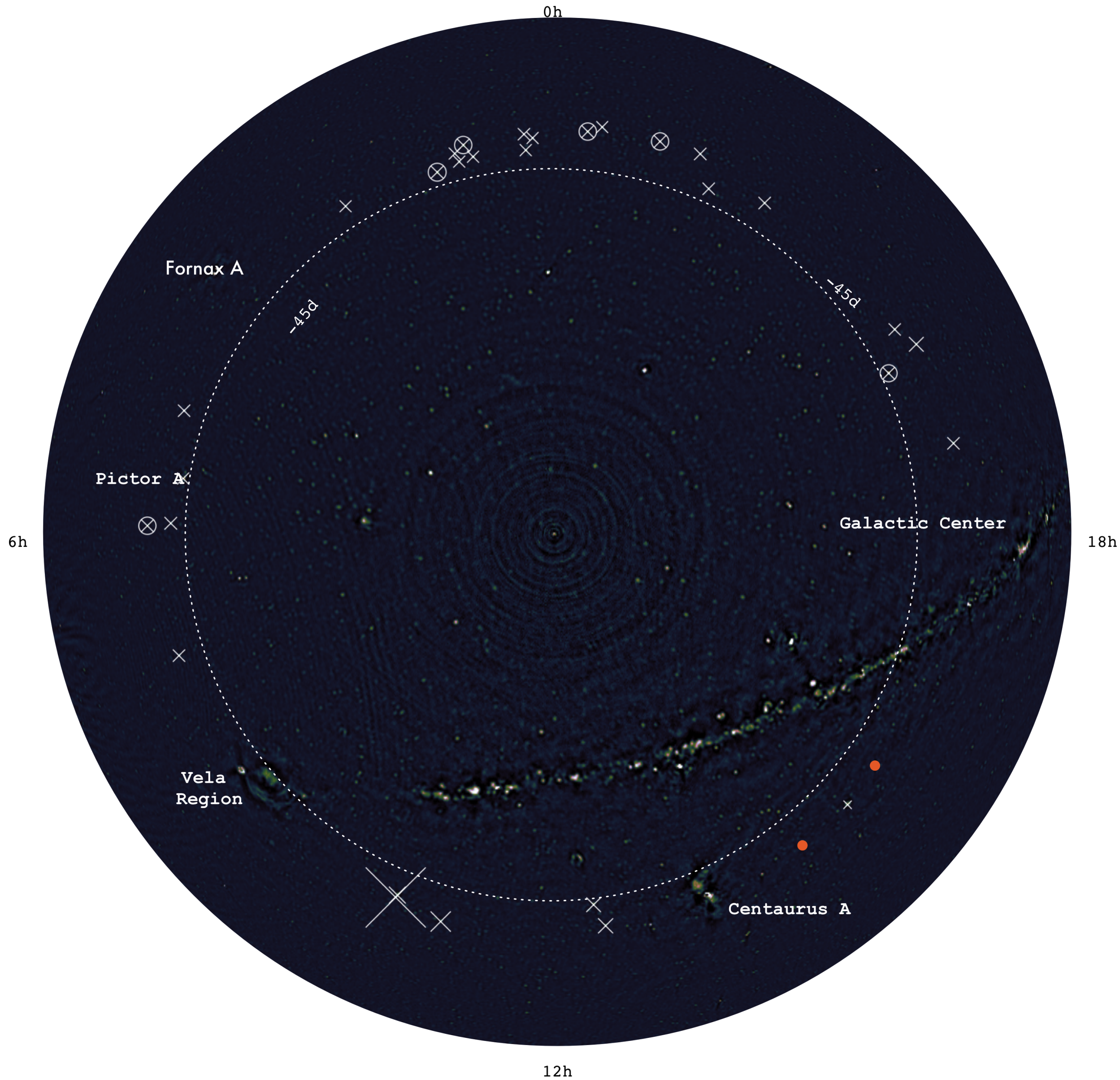

Fig. 15.— A PAPER map of the radio sky centered on the south pole showing relative positions of targeted sources. The map was made using the July half of the data used in this catalog using the procedure described in Jacobs et al. (2011) to produce a lightly CLEANed map. The circular artifact around the south Celestial pole is due to residual instrumental cross-talk and appears to be highly localized below declinations of 75°where PAPER's sensitivity is small. x's mark measured source locations and have size scaled by dis-agreement with prior data (inverse "improvement index" from §5). Smaller indicates better agreement with past data. Orange dots indicate sources with no model overlap at 76% 13.

Table 2. Spectral fits for 31[1] MRC sources. Before and after the addition of PAPER data. 90% agree well with prior measurements and demonstrate increased precision over previous measurements. Full table available online.

			PAPER + Catalog				Catalog[2]				
Name	Ra deg	Dec deg	$S150$ Jy	ΔS Jy	α –	$\Delta\alpha$ –	$S150_p$ Jy	ΔS_p Jy	α_p –	$\Delta\alpha_p$ –	Imp.[3] –
Pictor A	80.09	-45.78	381.88	5.36	-0.76	0.01	392.63	21.18	-0.77	0.04	0.942
0003-428	1.68	-42.5	12.24	0.61	-0.86	0.11	12.42	2.75	-0.86	0.19	0.636
0007-446	2.8	-44.3	19.17	0.82	-1.02	0.11	18.08	4.0	-0.98	0.19	0.704
0008-421	2.89	-41.81	5.68	2.13	-0.03	0.22	9.67	4.11	-0.32	0.24	0.31
0039-445	10.7	-44.16	24.78	0.91	-0.86	0.12	22.6	4.96	-0.78	0.19	0.801
0043-424	11.72	-42.05	41.69	1.27	-0.77	0.1	36.14	4.93	-0.69	0.12	0.34
0048-447	12.87	-44.4	13.24	0.64	-0.99	0.12	13.37	2.81	-0.99	0.19	0.657
0049-433	13.22	-43.03	18.99	0.84	-0.91	0.11	21.2	4.58	-1.01	0.2	0.754
0103-453	16.48	-45.02	25.73	1.07	-1.11	0.1	21.75	2.85	-1.04	0.12	0.177
0201-440	31.05	-43.76	11.71	0.66	-0.6	0.12	10.19	6.72	-0.5	0.44	2.805
0438-436	70.17	-43.53	7.51	0.38	-0.14	0.08	8.35	1.13	-0.21	0.1	0.305

[1]0008-421 is self-absorbed at 150MHz and is not listed here, while 1 did not have sufficient catalog data for a spectral fit and was also excluded

[2]MCMC fits to prior catalog data, before addition of PAPER measurements

[3]SED figure of merit change times confidence overlap, a measure of accuracy and precision. Higher value indicates an increase in both model fit precision and accuracy.

de Oliveira-Costa, A., Tegmark, M., Gaensler, B. M., Jonas, J., Landecker, T. L., & Reich, P. 2008, Monthly Notices of the Royal Astronomical Society, 388, 247, (c) Journal compilation © 2008 RAS

Foreman-Mackey, D., Hogg, D., Lang, D., & Goodman, J. 2012, eprint arXiv:1202.3665

Furlanetto, S. R., Oh, S. P., & Briggs, F. H. 2006, Physics Reports, 433, 181, elsevier B.V.

Hogg, D. W., Bovy, J., & Lang, D. 2010, eprint arXiv, 1008, 4686, a chapter from a non-existent book

Jacobs, D. et al. 2011, The Astrophysical Journal, 734, L34

Jacobs, D., Bowman, J., & Aguirre, J. 2013a, arXiv, astro-ph.CO, 10 pages, 10 figures, submitted to ApJ

—. 2013b, eprint arXiv, 1303, 2107, 10 pages, 10 figures, submitted to ApJ

Kuehr, H., Witzel, A., Pauliny-Toth, I., & Nauber, U. 1981, Astronomy and Astrophysics Supplement Series, 45, 367

Large, M. I., Mills, B. Y., Little, A. G., Crawford, D. F., & Sutton, J. M. 1981, ROYAL ASTRON. SOC. MONTHLY NOTICES V.194, 194, 693, a&AA ID. AAA029.002.002

Liu, A., Tegmark, M., & Zaldarriaga, M. 2009, Monthly Notices of the Royal Astronomical Society, 394, 1575, (c) Journal compilation © 2009 RAS

Mackay, D. J. C. 2003, Information Theory

Moore, D. F., Aguirre, J. E., Parsons, A. R., Jacobs, D. C., & Pober, J. C. 2013, eprint arXiv, 1302, 876, 29 pages, 12 figures

Morales, M. F. & Wyithe, J. S. B. 2010, Annual review of astronomy and astrophysics, 48, 127

Offringa, A. R., de Bruyn, A. G., & Zaroubi, S. 2012, Monthly Notices of the Royal Astronomical Society, 422, 563

Otrupcek, R. & Wright, A. 1991, Proceedings of the Astronomical Society of Australia, 9, 170

Paciga, G. et al. 2013, eprint arXiv:1301.5906

—. 2011, Monthly Notices of the Royal Astronomical Society, 413, 1174

Parashare, C. R. 2011, ProQuest Dissertations And Theses; Thesis (Ph.D.)–University of Virginia, 55

Parsons, A. et al. 2010, The Astronomical Journal, 139, 1468

Parsons, A., Pober, J., McQuinn, M., Jacobs, D., & Aguirre, J. 2012, The Astrophysical Journal, 753, 81

Parsons, A. R. & Backer, D. C. 2009, The Astronomical Journal, 138, 219

Parsons, A. R. et al. 2013, arXiv, astro-ph.CO

Perley, R. A., Roser, H.-J., & Meisenheimer, K. 1997, Astronomy and Astrophysics, 328, 12

Pober, J. C. et al. 2013, eprint arXiv, 1301, 7099, 6 pages, 5 figures, submitted to ApJL

—. 2012, The Astronomical Journal, 143, 53

Press, W. 1997, Unsolved Problems in Astrophysics, 49

Pritchard, J. R. & Loeb, A. 2012, Reports on Progress in Physics, 75, 6901

Sivia, D. & Skilling, J. 2006, citeulike.org

Slee, O. 1995, Australian Journal of Physics, 48, 143, d

Stefan, I. I. et al. 2012, eprint arXiv, 1212, 1624

Tingay, S. et al. 2013, Publications of the Astronomical Society of Australia, 30, 7

Vollmer, B., Gassmann, B., Derriere, S., Boch, T., & Louys, M. 2010, arxiv.org

Williams, C. L. et al. 2012, The Astrophysical Journal, 755, 47

Wills, B. J. 1975, Australian Journal of Physics, 38, 1, a&AA ID. AAA014.141.131

Yatawatta, S. et al. 2013, Astronomy & Astrophysics, 550, 136

This preprint was prepared with the AAS LaTeX macros v5.2.